Photogating effect as a defect probe in hydrogenated nanocrystalline silicon solar cells

Hongbo B. T. Li (李洪波),[a] Ruud E. I. Schropp, and Francisco A. Rubinelli[b]
Faculty of Science, Debye Institute for Nanomaterials Science, Nanophotonics-Physics of Devices, Utrecht University, P.O. Box 80.000, 3508 TA Utrecht, The Netherlands

(Received 1 January 2010; accepted 2 May 2010; published online 13 July 2010)

The measurement of the spectrally resolved collection efficiency is of great importance in solar cell characterization. Under standard conditions the bias light is a solar simulator or a light source with a similar broadband irradiation spectrum. When a colored blue or red bias light is used instead, an enhanced collection efficiency effect, in the literature known as the photogating effect, can be observed under certain conditions. While most of the published reports on such effect were on solar cells with amorphous silicon based absorber layers, we have shown that the enhanced collection efficiency could be also present in thin film silicon solar cells where hydrogenated nanocrystalline silicon (nc-Si:H) is used as the absorber layer. In this article we present detailed experimental results and simulations aiming at a better understanding of this phenomenon. We show that the collection efficiency is strongly dependent on the intensity of bias light and the intensity of the monochromatic light. These experimental results are consistent with the computer predictions made by our code. We also show that the photogating effect is greatly enhanced when nanocrystalline silicon cells are built with an improperly doped p-layer or with a defective p/i interface region due to the reduced internal electric field present in such cells. The existence of this effect further proves that carrier transport in a nc-Si:H solar cell with an i-layer made close to the phase transition regime is influenced to a large extent by drift transport. The study of this effect is proposed as an alternative approach to gain a deeper understanding about the carrier transport scenarios in thin film solar cells, especially nanocrystalline silicon solar cells. © *2010 American Institute of Physics*. [doi:10.1063/1.3437393]

I. INTRODUCTION

Hydrogenated nanocrystalline silicon (nc-Si:H), also called microcrystalline silicon, contains 10–20 nm sized silicon crystallites embedded in amorphous silicon (a-Si:H) tissue. Compared to conventional a-Si:H, nc-Si:H shows higher mobility and electrical stability. In the last decade considerable effort has been put in developing devices based on nc-Si:H in applications such as solar cells that are now moving rapidly toward mass production. Despite of this success some fundamental properties of this material, such as the electrical conduction mechanism, is not completely clear due to the multiphase nature of the material structure. However, it has been shown that solar cells made by depositing nc-Si:H under certain controlled conditions can be well described by simulation codes based on only one-dimensional calculation,[1,2] indicating similarity of nc-Si:H devices compared to that of conventional a-Si:H.

The name "photogating" (PG) was proposed by the group at Pennsylvania State University in 1992 (Ref. 3) for the anomalously high quantum efficiencies (QE) observed in amorphous silicon based structures. The PG effect was first observed in the 1980s when QE over unity were reported for a-Si:H Schottky barriers.[4] The main characteristic of this effect is the observation of unusually high values either at red wavelengths in the QE measured under blue bias light (BBL) or at blue wavelengths in the QE measured under red bias light (RBL).[5] Most of the reports about the PG effect published in the literature refer to amorphous silicon (a-Si:H) based thin film structures.[3–7] In single p-i-n solar cells the effect can be observed in samples degraded by light soaking,[3,5] or in an a-Si:H p-i-n structure with a very thick (up to a few micron) i-layer.[7] In Schottky barriers it was observed also in the annealed state at moderate forward voltages.[6] Enhanced QE were not only measured in thin film silicon devices but also on other structures like CdS/CdTe solar cells.[8–10]

Recently, we have reported for the first time the observation of enhanced quantum efficiency in nc-Si:H n-i-p cells measured with colored bias light, and have shown some preliminary experimental data and simulations about the dependence of this enhancement on the bias light used in the measurement.[11] In this article we present more detailed experimental results as well as simulation work that was carried out to obtain a deeper understanding of this effect. Using the computer code D-AMPS (Ref. 12) (analysis of microelectronic and photonic structures+new developments), we were able to find a good correlation between simulations and the experimental results. Further, we show the influence of cell deposition parameters on this effect, and discuss the use of the PG effect for solar cell optimization. Because of the unnaturally high values of the external collection efficiency (ECE) observed in the cells discussed in this article, we in-

[a]Tel.: +31 30 2532345. FAX: +31 30 2543165. Electronic mail: h.li@uu.nl.
[b]Present address: INTEC, Universidad Nacional del Litoral, Güemes 3450, 3000 Santa Fe, Argentina.

troduce the term "apparent collection efficiency" (ACE) in order to describe these values.

II. EXPERIMENTAL DETAILS

The cells involved in this study have the following n-i-p structure: Substrate/rough Ag/ZnO back reflector/n-type nc-Si:H/intrinsic nc-Si:H/buffer/p-type nc-Si:H/ITO/Au (grid-lines), with an active cell area of 0.13 cm^2. All silicon layers were deposited in the multichamber UHV system of Utrecht University called PASTA. Intrinsic i-layers were deposited by the Hot-Wire Chemical Vapor Deposition (HWCVD) technique. Two 0.5 mm tantalum (Ta) filaments were used. The filament current was adjusted to be 10.5 A, with a calibrated filament temperature of around 1850 °C, which results in a substrate temperature of 250 °C.[13] The $H_2/(H_2+SiH_4)$ gas flow ratio R_H is typically fixed as 0.952. Doped layers (p- and n-type silicon) were deposited by plasma enhanced CVD in separated chambers. The substrates used were either conformal Ag/ZnO-coated Asahi U-type TCO glass, or Ag deposited at high temperatures (for proper roughness) with a ZnO coating made in house by sputtering.

Structural characterization was done by Raman scattering spectroscopy and cross-sectional transmission electron microscopy (XTEM) both on solar cells and on individual thin films. Raman measurements on solar cells were performed with the laser beam (wavelength 514 nm) focused on the p-layer side of the sample over the area without the ITO coating. Cross-sectional TEM investigations were performed with a Philips Tecnai 12 electron microscope. A spectral response (SR) setup that allows for simultaneously applying bias light and bias voltage was used to measure the ECE of the solar cells. The light source used to produce the bias light as well as the monochromatic light was a xenon lamp. A short-pass filter KG1 was placed in the bias beam to filter out the extra infrared light. The colored bias lights were obtained by filtering the bias light with a 3 mm thick short pass filter BG23 (with a high transmittance in the wavelength range between 380 and 520 nm) and with a 2 mm thick long pass filter RG630 (transparent for light with wavelength >630 nm), respectively. The *total (integrated)* photon fluxes of the bias light beam were around $4(7)\times10^{16}$ $cm^{-2}\,s^{-1}$ for blue (red) bias light. The *spectral flux density* of the monochromatic beam, defined as the spectral flux per unit wavelength, varies with the wavelength. It was estimated to be $\sim3\times10^{13}$ $cm^{-2}\,s^{-1}\,nm^{-1}$ at ~650 nm. Light with this and higher wavelengths is practically uniformly absorbed in the solar cell. The bandwidth of the monochromator is estimated to be around 10 nm. The intensity of the white bias light (with the KG1 filter,) was around 100 mW/cm^2 and was kept constant. The light intensity was varied using a set of neutral density filters in the beam path. Current density-voltage (J-V) characteristics were measured with a dual-beam solar simulator (WACOM) while the cells were kept at 25 °C. To avoid possible misinterpretations due to inherent differences between the short circuit current (J_{sc}) from J-V measurements and the integrated J_{sc} from ECE measurements, unless mentioned otherwise, the former J_{sc} was corrected with respect to the integrated J_{sc} using the ECE plot obtained under the standard white light measurement and the tabulated AM1.5 spectrum.[14] We denote this current as J_{sc}^{SR}.

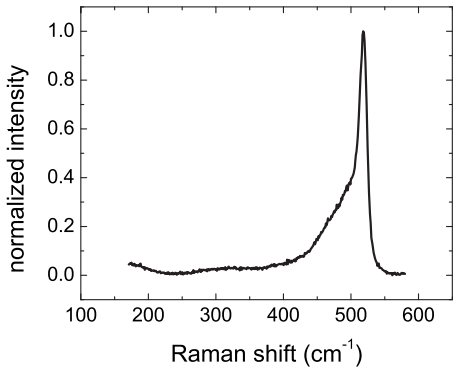

FIG. 1. Raman scattering spectra of a nc-Si:H n-i-p cell obtained with the laser incident on the p-layer side of the cell.

III. EXPERIMENTAL RESULTS

A. Structure of nc-Si:H solar cells with hot-wire CVD deposited i-layer

The structure of nc-Si:H solar cells was studied with Raman scattering spectroscopy. Figure 1 shows the typical Raman scattering spectrum obtained for our samples. Clearly, the spectrum shows a pronounced crystalline silicon TO peak at 520 cm^{-1} that indicates the presence of a nc-Si:H structure. Due to the limited penetration depth of the incident laser the Raman scattering spectra only gives information on the material near the p-layer side of the n-i-p structure. To obtain information on the entire i-layer of the cell, XTEM specimens of samples deposited under identical conditions were prepared. Figure 2 shows the bright field TEM picture for such a sample. The dark edge on the lighter, lower left corner is the ~80 nm thick ITO coating, while the dark edge on the upper right corner of the image is the Ag/ZnO coated glass substrate. Adjacent to each of these two sides the ~20 nm thin p-layer (adjacent to the ITO coating) and n-layer (adjacent to the substrate) are discernible. In the middle part of the picture the ~1.3 μm thick nc-Si:H i-layer can be clearly seen.

B. Observation of enhanced ACE

Figure 3 shows typical ACE characteristics of a cell exhibiting enhancements when colored bias light was used. The

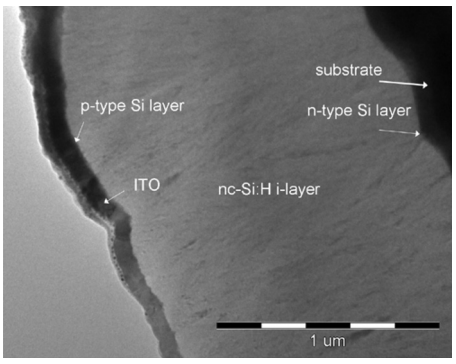

FIG. 2. XTEM picture of the nc-Si:H n-i-p cell shown in Fig. 1.

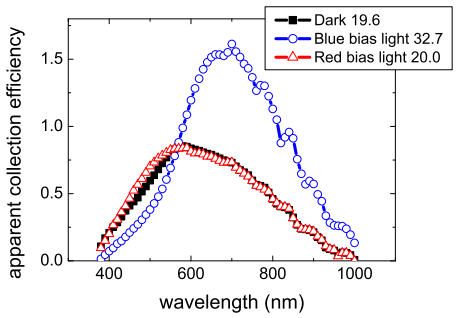

FIG. 3. (Color online) ACE of a nc-Si:H n-i-p cell measured with colored bias light. Solid squares: the cell is measured under dark conditions; open circles: with BBL; up triangles: with RBL. The numbers in the legend show the integrated current density in mA/cm^2 under AM1.5 illumination.

curve marked with squares is the measurements performed in the dark and at short circuit conditions. The integrated current density J_{sc}^{SR} of 19.24 mA/cm^2 obtained by measuring the spectral response under white light conditions (not showed in Fig. 3), i.e., using the tabulated AM1.5 solar spectrum, has an appropriate value for a ~1.3 μm thick n-i-p nc-Si:H cell on an Ag/ZnO-coated Asahi U-type TCO substrate. Under the BBL (see in Fig. 3 the curve with circles) a greatly enhanced ACE is observed in the long wavelength (λ) region of the spectrum (in the range between 550 and 1000 nm) with a peak value of ~1.61 at around 700 nm. Simultaneously, the ACE curve in the short wavelength region ($\lambda < 550$ nm) shows lower values than under the equilibrium condition. The integrated current density amounts to a value of 32.7 mA/cm^2, which is ~70% higher than the measured current under dark conditions. When instead the red RG630 filter is positioned in the bias light path (see the curve with upward triangles in Fig. 3) an enhanced blue response and a slightly decreased red response are observed. For the sake of brevity we will concentrate our discussion on the ACE observed under BBL illumination. We will explore the ACE obtained under other illumination conditions in future contributions.

C. Light intensity dependence of the ACE

The observation of the strongly enhanced ACE implies that besides the current generated by the monochromatic probe light, there must be extra charge carriers that are collected by the lock-in amplifier. Without any active electronic-optical conversion effect the ECE is not expected to be greater than unity. The fact that the ACE plots measured under standard light bias conditions show normal values (namely ECE by definition) suggests that this extra current in the red region of the spectrum may be related to the use of the BBL. To test this hypothesis various neutral density filters were interposed in the bias light path in combination with the blue filter BG23. The resulting ACE responses are shown in Fig. 4. Clearly, the height of the ACE peak decreases with decreasing bias light intensity. This indicates that the enhanced response is indeed related to the BBL used. The physics behind this phenomenon was explored with computer device simulations.

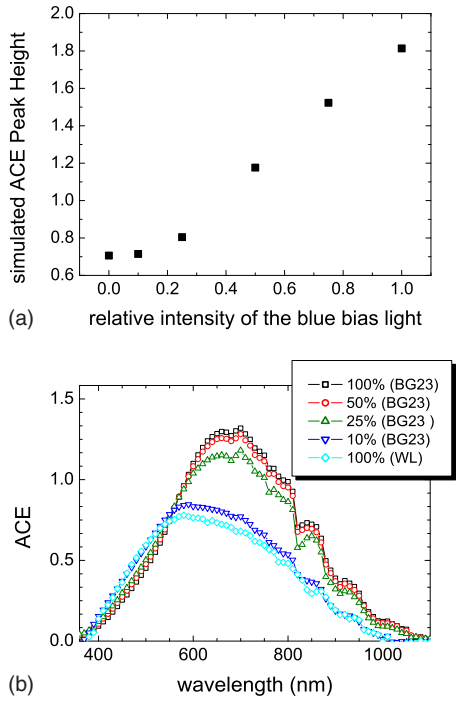

FIG. 4. (Color online) Dependence of the ACE with respect to the bias light intensity. (a) Simulated ACE peak height. The experimentally determined intensity of BBL is set as 100%. (b) Experimental result (nn %): transmittances of neutral density filters; BG23: type of blue filter used to generate the blue bias beam; WL: white light, no color filter was used.

IV. D-AMPS ANALYSIS

The computer code D-AMPS was used to study the PG effect. D-AMPS is an updated version of the program AMPS (analysis of microelectronic and photonic devices) developed at the Pennsylvania State University. The letter D stands for new developments that were implemented by the third author of this manuscript (amphoteric states, defect pool model, Pool–Frenkel effect, light interference, carrier tunnelling, etc.).[12]

A. Principle of ECE measurement

Before we further discuss the strongly enhanced ACE in more detail, it is worth describing briefly the principle of the ECE measurement in the presence of bias light. In these experiments a weak and chopped monochromatic probe beam (wavelength λ) of photon flux $\phi_{ML}(\lambda)$ is incident on the sample in conjunction with a much stronger dc bias light (BL) of photon flux ϕ_{BL}. The ECE is then obtained by synchronously detecting the ac component $\Delta J(\lambda)$ of the resulting photocurrent density with a lock-in amplifier. Thus,

$$ECE = \Delta J(\lambda)/e\phi_{ML}(\lambda), \quad (1)$$

where e is the electron charge. The assumption implicitly contained in this measurement is that all photocarriers carrying $\Delta J(\lambda)$ were generated by the probe beam light. While this is generally the case under white bias light conditions or in the absence of bias light, this assumption appears invalid when using colored bias light.

TABLE I. Input parameters used in D-AMPS for the Si layers of the nc-Si:H p-i-n structure.

Input parameter	p	i	n
Thickness (nm)	20	1300	27
Effective band gap (mobility gap/optical gap) (eV)	1.2	1.25/1.2	1.2
Effective density of states N_c, N_v (cm^{-3})	3×10^{19}	3×10^{19}	3×10^{19}
Electron/hole mobility (cm^2/Vs)	40/4	$100\sim10/10\sim1$ for experimental fitting: 40/4	40/4
Carrier capture cross section ($\sigma_{CH/NE}$) (cm^2)	$5\times10^{-14}/5\times10^{-15}$	$7.5\times10^{-15}/7.5\times10^{-16}$	$5\times10^{-14}/5\times10^{-15}$
Tail characteristic energy E_D-E_A (meV)	35–23	35–23	35–23
Amphoteric-like Gaussians ($D^+/D^0/D^-$)			
Density of states (cm^{-3})		$(0.2\sim100)/(0.1\sim50)/(0.2\sim100)\times10^{15}$ for experimental fitting: $(1\sim10)/(0.5\sim20)/(1\sim10)\times10^{15}$	
Peak position of donor Gaussian from E_v (eV)		0.3/0.6/0.9	
Width (eV)		0.1/0.1/0.1	
Correlation energy (eV)		0.2	

B. Input parameters for D-AMPS

Using D-AMPS, we evaluated n-type nc-Si:H/ intrinsic nc-Si:H/ p-type nc-Si:H/ITO cell structures on stainless steel (SS) or glass substrates, both with and without textured Ag/ZnO back reflector. The baseline input parameters used in this manuscript were taken from previous research done by Strengers *et al.*[2] on our nc-Si:H n-i-p cells. Three amphoteric-like Gaussians, D^+, D^0, and D^-, were adopted to model the density of mid-gap states in the nc-Si:H layers.[15] The areas, widths, and heights of the Gaussians are shown in Table I. The dangling bond (DB) densities adopted in doped layers are based on experimental results and on typical values extracted from the literature. Important parameter values, such as effective band gap, defect density distribution, carrier mobilities of the intrinsic nc-Si:H materials were adjusted in order to produce simulations that describe our experimental results over a broad range of conditions. Note that the DB density parameters found by Strengers *et al.*[2] were in the lower part of the range listed in Table I ($\sim2.5\times10^{15}$ cm^{-3}). The free carrier mobilities and the density of states are specified within two ranges in Table I: a wide range, to explore the dependence of the ACE on these key parameters, and a narrow range, to closely reproduce the experimental trends of the samples studied in this paper. Table I also shows the other essential parameters used for the simulations. The back and front layers, i.e., ZnO and ITO, respectively, are treated only optically, while the band offsets between ITO/p interfaces and ZnO/n interfaces are included in the description of the electrical transport. The optical properties of ITO and ZnO, $n(\lambda)$ and $k(\lambda)$, were obtained from the reflection and transmission spectra measured on materials deposited on polished crystalline silicon wafers. The spectral intensities of various bias light conditions were extracted from experimentally detected light spectra.

C. Simulation results: Sensitivity study

Mid-gap defect states in the intrinsic layer were assumed to be homogeneously distributed over the entire thickness of the cell, which was determined to be 1.3 μm from electron microscopy images[16] (Fig. 2). The basic assumption of this work is that although the structure of nc-Si:H is inhomogeneous in nature, it can be described by an effective electrical model with a basic band structure similar to that of a-Si:H alloys. The assumption of these features is justified by various results in the literature.[17–19] We thus assume a mobility band gap with exponential band tails at the band edges and defects located between the band edges with distributions that can be described by Gaussians. We use a band gap value of 1.2 eV to describe both the intrinsic and doped nc-Si:H and vary the mobilities in a wide range to study their effect on PG, and later we fix the electron and hole mobilities to be 40 cm^2/Vs and 4 cm^2/Vs, respectively, for intrinsic nc-Si:H. Properties of the doped layers and of the ITO and ZnO layers were also assumed to be homogeneous. The sensitivity of ACE was explored with respect to different electrical parameters, such as the effective band gap, the defect density distribution, and the electron and hole mobilities of the i-layer. It was found that the ACE values are very sensitive to free carrier mobilities and to the mid-gap state density present in the intrinsic layer. Small changes in these input parameters led to significant changes in the predicted ACE. Figure 5 show the simulated ACE curve for different values of the hole mobility (μ_p) and of the electron mobility (μ_n) assuming that the density of DB in the intrinsic layer is $\sim2.5\times10^{16}$ cm^{-3}. An increase in the ACE is predicted for higher electron mobilities (assuming a hole mobilities of 5 cm^2/Vs) and for lower hole mobilities (assuming an electron mobilities of 50 cm^2/Vs). The intensity of the BBL in the simulations was set equal to the experimentally determined light intensity. The other parameters used to generate Fig. 5 are listed in Table I. Our main objective is to reproduce with computer simulations the trends experimentally observed and discuss the physics behind the observation of these anomalous responses. Although there is no attempt in this paper to match exactly the ACE curves, the high sensitivity of the ACE to small changes in the illumination conditions and in the electrical quality of the deposited samples provide a good way to test the reliability of our input parameters. It is also important to mention that enhanced ACE are also predicted by D-AMPS at red wavelengths for low DB densities like $\sim5\times10^{15}$ cm^{-3} but their ACE peaks are below unity.

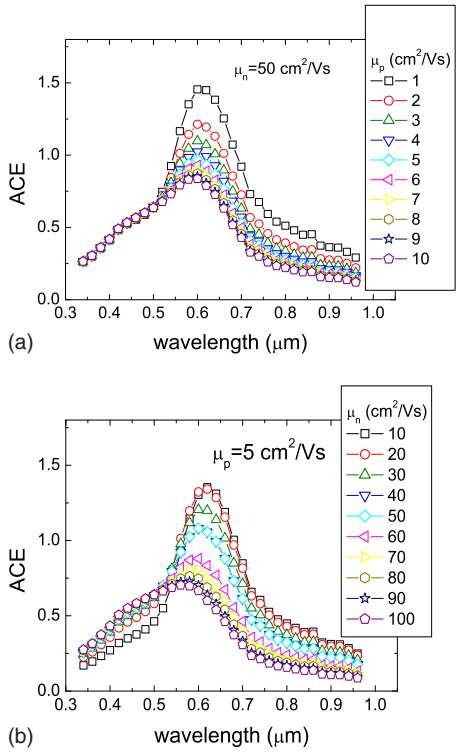

FIG. 5. (Color online) Simulated ACE spectra of the n-i-p cell assuming a homogeneous defect density profile along the i-layer thickness (Density of States=2.5×10^{16} cm^{-3}). (a) μ_n is fixed at 50 cm^2/Vs, μ_p is varied as $1,2,\ldots,10$ cm^2/Vs; (b) μ_p is fixed at 5 cm^2/Vs and μ_n is varied as $10,20,\ldots,100$ cm^2/Vs.

In Fig. 6, the ACE peak values that can be found at around 600–620 nm wavelength from our simulation are plotted with respect to the DB density for different values of the free carrier mobilities μ_n and μ_p. The defect density was varied between 5×10^{14} and 2×10^{17} cm^{-3}. These curves were generated for a nc-Si n-i-p solar cell on a SS substrate without back reflector. In order not to obscure the PG effect by optical enhancement features, the simulated device structure does not contain the Ag/ZnO back reflector layers present in the characterized sample. Figure 6 clearly reveals that the enhanced ACE, the magnitude of its peaks, and the minimum DB density required to generate the PG effect are strong functions of the free carrier mobilities. In Sec. IV F we will show that the ACE is also a function of the intrinsic layer thickness. The fact that no light scattering back reflector was used to produce these figures indicate that light enhancing elements are not essential to generate the enhanced ACE (though they do modify to some extent the shape of the ACE curves). Scattering at the front ITO/p interface also affects the shape of the SR because the BBL becomes more strongly absorbed near the p/i interface and more weakly absorbed in the bulk with respect to samples with flat interfaces. Except for this, the PG effect is essentially an electrical phenomenon.

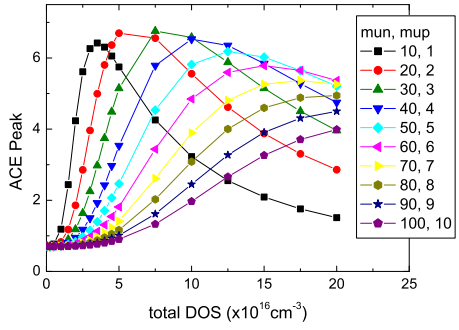

FIG. 6. (Color online) Dependence of the peak value of the ACE on the hole mobility μ_p and on the electron mobility μ_n. The values of their counterpart (μ_p and μ_n, respectively) are kept unchanged and shown in the legend area. The i-layer thickness is kept constant as 1.3 μm.

Figure 6 indicates that for the solar cell studied in this paper that has an i-layer thickness of 1.3 μm and for typical nc-Si:H mobilities μ_n and μ_p of 40 cm^2/Vs and 4 cm^2/Vs, respectively, the most pronounced ACE are predicted for DB densities in the range 7×10^{16}–1.7×10^{17} cm^{-3}, with ACE peak values of over 500%. On the other hand, for high quality materials with DB densities in the range $\sim10^{15}$ cm^{-3} or below, the PG effect does not emerge for a $\sim$1.3 μm thick cell in our simulations, unless the combination of the bias and the probe light are modified. Since the purpose of this paper is to understand the physics of the PG effect in nc-Si:H solar cells, we do not spend effort to maximize the ACE peak height for each device by varying measurement conditions. That will be the topic for future publications.

All these results point out that the final shape of the enhanced ACE observed in nc-Si:H n-i-p cells solar cells is highly influenced by drift phenomena even though nc-Si:H is a material with higher free carrier mobilities than a-Si:H. Hence trapping and field changes introduced by the BBL and by the monochromatic beam are analyzed in Sec. IV D following an approach similar to that used in a-Si:H based devices.[3,6]

D. Analysis: Electrical field distribution

Due to the existence of electrical defects or gap states the internal electric field in the intrinsic layer of a nc-Si:H n-i-p cell is not homogeneously distributed. This can be seen in Fig. 7(a), where the simulated internal electrical field profile under short circuit conditions and at thermodynamic equilibrium are shown. The electric field at equilibrium (solid line) is stronger near the p/i and i/n interfaces and weaker in the middle part of the i-layer. The electric field profile resembles the distribution found in thick amorphous n-i-p solar cells where two depletion regions separated by a quasineutral region are formed: one for electrons and one for holes at the front and back regions of the intrinsic layer, respectively. When the cell is illuminated defects will act as trapping centers for photogenerated electrons and holes. Trapping by gap states could give rise to significant changes in the final shape of the charge densities and electric field profiles with respect to the situation found at equilibrium. This can be seen in Fig. 7(a) and Fig. 7(b), where we compare the field and the space charge profiles under equilibrium and under different illumination conditions. The field profile under red illumination [see Fig. 7(a), the dashed line], which is uniformly absorbed in the intrinsic layer, shows its minimum intensity shifted to the rear side of the cell with respect to the field under dark conditions [Fig. 7(a), the solid line].

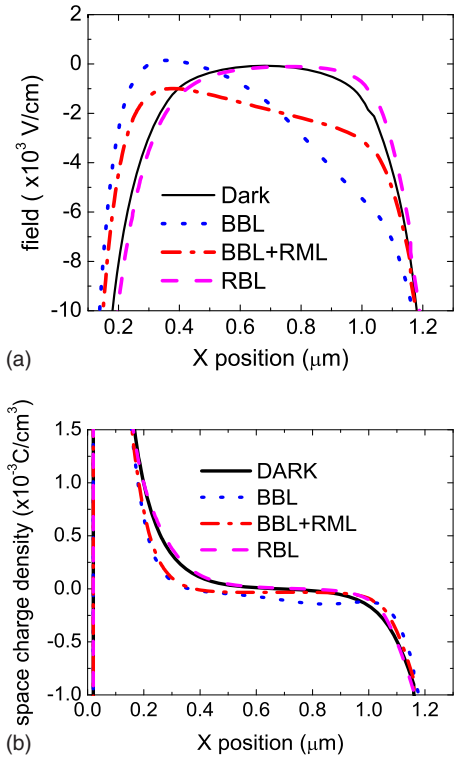

FIG. 7. (Color online) Distributions of the electric field (a) and space charge (b) inside the intrinsic layer at the short circuit conditions. BBL: under blue bias light; RBL: under red bias light; BBL+RML: under blue bias and red monochromatic light. Dark: thermodynamic equilibrium conditions.

The field redistribution consists of a reinforcement near the front interface and a deterioration in the bulk, as a result of the preferential trapping of photogenerated holes near the p/i interface and of photogenerated electrons near the i/n interface after they have drifted due to the field. The lower mobility of holes makes trapping of photogenerated holes and its impact on the field redistribution more significant than trapping of photogenerated electrons.

When the cell is illuminated with a strong blue bias light (denoted as BBL in Fig. 7, created from the AM1.5 spectrum with a blue filter, *total* photon flux around 4×10^{16} cm^{-2} s^{-1}), most of the incident photons are absorbed in the front part of the cell due to the high absorption coefficient of intrinsic nc-Si:H at short wavelengths. The field redistribution in this case is practically opposite to that under red bias light (denoted as RBL): the field is weakened in the front part of the i-layer, with a minimum close to zero, and reinforced at the rear side of the cell, compared to the field under dark conditions [see Fig. 7(a)]. This redistribution of the electrical field is introduced by trapping over the whole i-layer thickness of the electrons generated by the BBL. Holes are generated by this bias light quite near the front contact and therefore they mostly exit the device before being trapped. A small fraction of holes may be trapped on their way out but they do not have any impact on the PG effect. It is worth noting that the area under the electric field profiles for different illumination conditions is identical at a given bias voltage. In other words, the deterioration of the electric field introduced by the BBL at the front part of the i-layer must be compensated by the reinforcement of the field at the rear part of the i-layer.

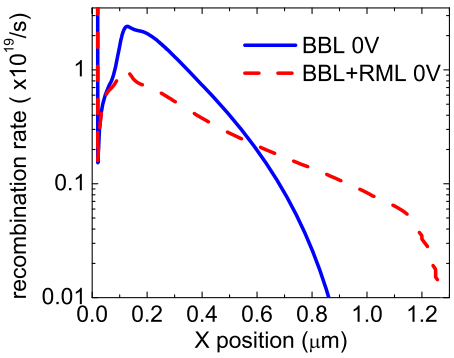

FIG. 8. (Color online) Comparison of the recombination rate profiles when only the BBL (solid line) is focused on the cell and when both the BBL and a weak red probe beam RML (dashed line) are present.

When a red modulated probe beam (denoted as RML) with the photon flux in the order of 6×10^{14} cm^{-2} s^{-1} is superimposed to the strong blue bias beam (BBL), these photons are nearly homogeneously absorbed in the i-layer. The simultaneous presence of the BBL and the RML will be named as the BBL+RML scenario. The RML beam reinforces the field in the front region of the i-layer and weakens the field in the back region of the i-layer. The largest influence is observed in the rear part of the i-layer where the BBL is not absorbed. In the front part of the device the space charge density is dominated by the BBL, which intensity is more than an order of magnitude higher than that of the monochromatic probe beam. This can be seen in Fig. 7(b). This modulating space charge distribution shown in Fig. 7(b) by the dashed-dotted line is doing so at the frequency of the optical chopper, resulting in a modulating field which is in phase with the incident monochromatic probe beam as shown in Fig. 7(a) by the dashed dotted line. Thus the weakened electric field in the front part of the i-layer by the BBL alone is significantly reinforced by the presence of the RML of the probe beam, although not completely to the extent to recover the field present under equilibrium conditions. Due to the dominating absorption of the strong BBL the change in the space charge distribution in Fig. 7(b) looks relatively small in the front region of the device compared to in the bulk. However, the redistribution of the electrical field in the front part of the i-layer has a significant influence on the carrier transport kinetics. The stronger electric field present under BBL+RML results in a significant decrease in the recombination rate in the front part of the cell, as can be observed in Fig. 8, as well as a decrease in the back diffusion of electrons toward the front contact. These reductions in the electrical losses give rise to an extra modulated current that is in phase with the modulated monochromatic light and thus it is detected by the lock-in amplifier. Simultaneously the reinforcement of the electric field in the front region of the device reduces trapping of photoelectrons, i.e., a fraction of the photocarriers generated by the dc bias light that would be trapped under BBL only are released to be part of the electrical current under BBL+RML illumination conditions.

The physical mechanisms responsible for the enhanced ACE values measured in nc-Si:H solar cells are similar to those present in the PG effect observed in amorphous silicon p-i-n and in Schottky barrier structures.[3,6] However in the present device the free-carrier mobilities are higher, the mobility gap is significantly narrower, and the device is considerably thicker. In a nc-Si:H solar cell, trapping is less severe but the recombination losses are more significant mainly due to the lower gap and to a smaller extent to the weaker electric field present in the bulk of the i-layer. This scenario leads D-AMPS to predict also the feasibility of observing PG effect under RBL that will be discussed in a future publication.

E. Light intensity dependence

Since the PG effect is closely related to the BBL used for the measurement, it is expected that the PG effect becomes more pronounced when the light flux of the BBL is higher. This can be seen in Fig. 4(a), where the simulated dependence of ACE peak height with respect to the bias light intensity is shown. Actually D-AMPS shows that the stronger the bias light is, the weaker the field profile becomes in the front region of the device. The red probe beam acting on a region with a smaller field would thus be able to release more carriers leading to a higher ACE. This was indeed observed in our experiment. Figure 4(b) exhibits the experimentally observed dependence of ACE on the bias light intensity, where a decrease in the bias light intensity indeed results in a decrease in the ACE peak height.

Our simulations also predict that with a decrease in the monochromatic beam intensity the PG effect is enhanced, as is seen in Fig. 9(a). To verify this, experiments were performed using three different probe beam intensities. The results are shown in Fig. 9(b). It can be seen that the ACE peak indeed increases with decreasing monochromatic beam intensity.

The enhancement of the PG effect for lower monochromatic light intensities can be explained by the interaction between the photogenerated carriers originating from the probe and bias beams individually. The RML, which is superimposed over the BBL, reinforces the electric field in the front region of the i-layer that is weakened by the BBL alone (the opposite happens in the back region of the i-layer). However, the stronger the intensity of the RML is, the more the electric field profile will be distorted from its original shape set up by the BBL alone. In the extreme case of very intense RML beams the PG effect will be lost, because we will then encounter a scenario similar to that found under RBL. It is worth keeping in mind that the ACE characteristic is the ratio between the synchronously detected current and the monochromatic beam intensity [see Eq. (1)], which in this case is the flux of the RML. Due to the opposite influence of the probe and bias beams on the field distribution, the lower the RML intensity is, the more carriers will be relatively gated out with respect to the incident RML flux. Therefore, a reduction in the ACE peak height with increasing modulated light intensity is predicted and observed.

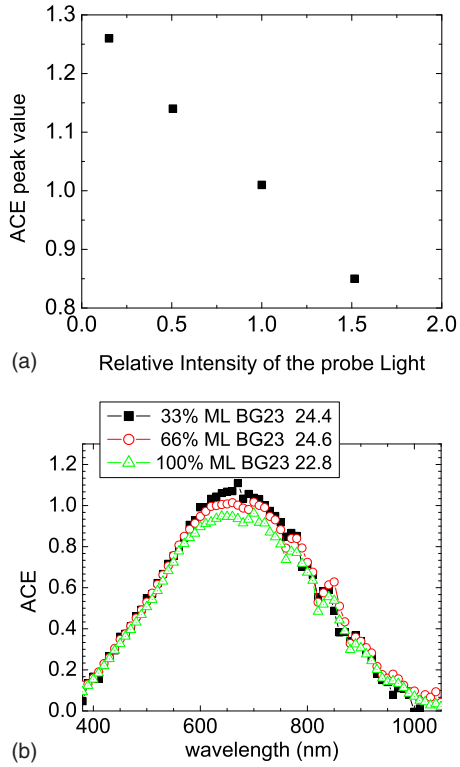

FIG. 9. (Color online) Dependence of the ACE with respect to the monochromatic light intensity. (a) Simulated ACE peak heights and (b) experimental results.

F. Thickness dependence

Above we have described how the PG effect depends on the internal field distribution. Therefore, cells incorporating the same i-layer material but with different thicknesses will likely influence the magnitude of the ACE values. The dependence of the ACE peaks with respect to the i-layer thickness of the cell was studied with simulations. With the mobilities μ_n, μ_p, and other parameters kept unchanged, the i-layer thickness was varied from 0.5 to 10 μm for a few values for the DB densities (total densities of 0.5, 1, 2.5, and 5×10^{16} cm^{-3}). The results are shown in Fig. 10 by solid dots. It can be seen that for the given material parameters there is an optimal thickness that maximizes the ACE, making it easier to observe the PG effect. Detailed simulations

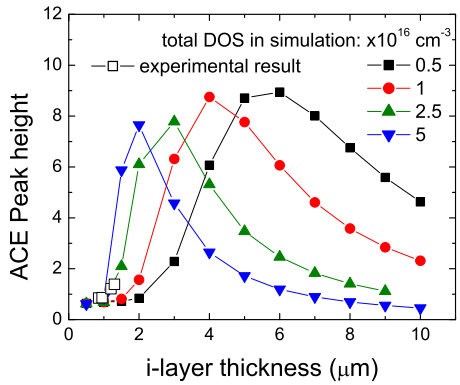

FIG. 10. (Color online) Dependence of the ACE with respect to the intrinsic layer thickness. Solid dots: simulated ACE peak heights. Open squares: comparison of the ACE maximums.

indicate that for a cell with a very thin i-layer (with a thickness far below the optimum) the stronger internal field present at equilibrium in the i-layer is more difficult to be modified by the BBL. The RML beam would also be less likely to effectively modulate the field tailored by the BBL. The carrier recombination losses that normally vary under the different illumination conditions will also be reduced by the presence of a stronger field. As a result, an ACE curve that is close to that obtained without using bias light (dark conditions) is observed. On the other hand, when the i-layer is too thick (much thicker than the optimum thickness), the released photocarriers mostly recombine at deep states before reaching the contacts due to the weaker electrical field. This also results in a decrease in the output current and therefore in the ACE peak height.

These predictions have then been tested experimentally using nc-Si:H cells with identical p and n layers but with variable i-layer thicknesses in the range of 700–1300 nm. The results are shown in Fig. 10 by open squares. It is observed that within the thickness range studied here, the PG peak values indeed vary with the i-layer thickness according to our prediction.

V. DISCUSSION

The consistency of the D-AMPS simulation with the experimental results indicates a large similarity of the unusually enhanced ECE of nc-Si:H solar cells with the PG effect, as previously observed in a-Si:H p-i-n structures.[3] We therefore conclude that the PG effect also describe the observed high collection efficiency under colored bias light in nc-Si:H cells.

The analysis made with D-AMPS suggests that a lowered electrical field generated by the combination of thick intrinsic layers and a significant density of trapping states in the intrinsic layer, or by one of these characteristics, are the key factors for observing a strong PG effect in the conventional quantum efficiency measurement condition. In a nc-Si:H cells with good i-layer quality the PG effect shall not be significant. However our experiments show that nc-Si:H cells with good i-layer quality can also exhibit the PG effect. Our ECE measurements with colored bias light showed that a PG effect can also be observed on such cells if the buffer/p/ITO region is unoptimized. It is likely that the internal field in such cells collapses in the bulk due to the barrier present in the front region, thus hindering carrier transport.[20] Postdeposition annealing treatment can largely remove this barrier and therefore results in recovery of the bulk electrical field. The ACE curves obtained on those cells before and after the annealing treatment indeed show a dramatic difference in the magnitude of the PG effect observed. One such example is depicted in Fig. 11, where the ACE of a sample with a nonoptimized front region was subjected to the annealing treatment. The ACE of the same sample prior to the anneal is presented in Fig. 3. Comparing the ACE characteristics measured before and after the annealing treatment the strong enhancement in the long wavelength region under the BBL (as seen in Fig. 3, with an ACE peak as high as 1.61) has been largely reduced (as shown in Fig. 11, with a ACE peak of ~0.87), and its J_{sc}^{SR} (21.13 mA/cm^2) is only slightly larger than that measured under white bias light (20.67 mA/cm^2). These figures strongly support the validity of our earlier hypothesis of the enhancement of the internal field after the postannealing treatment[20] on such cells.

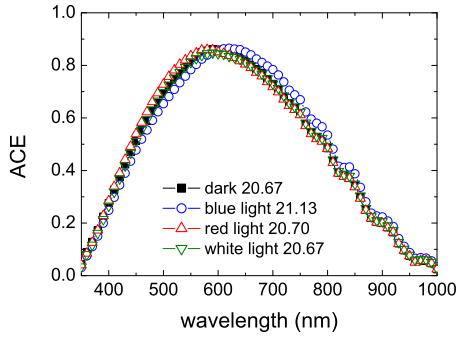

FIG. 11. (Color online) ACE characteristics of a cell after the postdeposition annealing treatment. The ACE curves measured before the treatment are shown in Fig. 3.

One important detail shown in Fig. 11 is that the i-layer in this cell was deposited at a constant hydrogen dilution rate R_H of 0.952. Raman and XTEM analyses on cells made on the same type of substrate and at the identical deposition conditions did not show crystallinity evolution of the i-layer, as was observed recently in hot-wire deposited nc-Si:H i-layers.[21] Fourier transform photocurrent spectroscopy analyses on this sample give an estimated value for the i-layer defect density of $\sim 3\times 10^{15}$ cm^{-3}. The AM1.5 J-V measurement on the as-deposited sample shows an efficiency of 4.80%, with J_{sc}, V_{oc} (open circuit voltage), and FF (fill factor) of 19.24 mA/cm^2, 0.47 V, and 0.531, respectively, indicating an inefficient collection of photogenerated carriers. After the postdeposition annealing treatment, the solar cell efficiency increased to 8.4%, with J_{sc}, V_{oc}, and FF of 23.6 mA/cm^2, 0.543 V, and 0.656, respectively. This measurement was performed with an illumination mask (the same as the mask used to deposit the ITO contact), but without correction of J_{sc} according to the ECE response.

The observation of the PG effect in nc-Si:H solar cells with i-layers made near the phase transition regime proves that carrier transport in such a cell is to a large extent determined by the internal electrical field in the i-layer. This is direct evidence for the importance of carrier drift mechanisms in such devices. It is worth noting that our simulations indicate that drift and diffusion currents in these materials could be comparable with some predominance of drift over diffusion.

VI. CONCLUSION

An enhanced quantum efficiency under BBL was observed for nc-Si:H single junction solar cells. Thickness and bias and monochromatic light intensity dependence of this effect are consistent with the computer simulated predictions and is similar to the PG effect that was previously observed in amorphous silicon based structures. The existence of this effect proves that carrier transport in a nc-Si:H solar cell made near the phase transition regime is to a large extent determined by the internal electrical field and thus carrier

drift is a significant transport mechanism. We therefore propose to extend the name "photogating" as observed in a-Si:H cells to describe this observed effect also in solar cells with nc-Si:H absorber.

To have an maximum energy output from nc-Si:H solar cells careful control of the quality of the doped layers and of their interfaces is needed. This optimizes the internal field in the i-layer and therefore this is of equal importance to the improvement of the electrical quality of the bulk intrinsic nc-Si:H layer. The measurement of the PG effect is proposed to be a useful method to study carrier transport of photovoltaic devices, especially those with nanocrystalline silicon absorbers.

ACKNOWLEDGMENTS

We thank our colleague C. H. M. van der Werf for sample preparation. The first author thanks Dr. Ales Poruba and Jakub Holovsky from Institute of Physics at Academy of Sciences of the Czech Republic for defect density estimations. The work was financially supported by the Netherlands Agency for Energy and the Environment (SenterNovem) of the Ministry of Economic Affairs.

[1]A. Sturiale, H. B. T. Li, J. K. Rath, R. E. I. Schropp, and F. A. Rubinelli, J. Appl. Phys. **106**, 014502 (2009).
[2]J. J. H. Strengers, F. A. Rubinelli, J. K. Rath, and R. E. I. Schropp, Thin Solid Films **501**, 291 (2006).
[3]J. Y. Hou and S. J. Fonash, Appl. Phys. Lett. **61**, 186 (1992).
[4]H. P. Maruska, M. C. Hicks, T. D. Moustakas, and R. Friedman, IEEE Trans. Electron Devices **31**, 1343 (1984).
[5]S. Bae and S. J. Fonash, J. Appl. Phys. **79**, 2213 (1996).
[6]F. A. Rubinelli, J. Appl. Phys. **75**, 998 (1994).
[7]C. Main, J.-H. Zollondz, S. Reynolds, W. Gao, R. Brüggemann, and M. J. Rose, J. Appl. Phys. **85**, 296 (1999).
[8]M. Gloeckler and J. R. Sites, J. Appl. Phys. **95**, 4438 (2004).
[9]G. Agostinelli, D. Batzner, and M. Burgelman, Proceedings of 29th IEEE PVSC Conference, p. 744 (2002).
[10]S. Hegedus, D. Ryan, and K. Dobson, Mater. Res. Soc. Symp. Proc. **763**, B9.5.1 (2003).
[11]H. B. T. Li, F. A. Rubinelli, J. K. Rath, and R. E. I. Schropp, 21st European PVSC Conference, Dresden, Germany, 4–9 September, 3DV3.51 (2006).
[12]F. A. Rubinelli, J. K. Rath, and R. E. I. Schropp, J. Appl. Phys. **89**, 4010 (2001).
[13]M. K. van Veen and R. E. I. Schropp, J. Appl. Phys. **93**, 121 (2003).
[14]"AM1 5 Global" spectrum is taken from Table 2c, column 1 and 6 from the article Spectral solar irradiance data sets for selected terrestrial conditions, by R. Hulstrom, R. Bird, and C. Riordan, Sol. Cells **15**, 365 (1985).
[15]E. Klimovsky, J. K. Rath, R. E. I. Schropp, and F. A. Rubinelli, Thin Solid Films **422**, 211 (2002).
[16]H. B. T. Li, R. H. Franken, J. K. Rath, and R. E. I. Schropp, Sol. Energy Mater. Sol. Cells **93**, 338 (2009).
[17]J.-H. Zhou, S. D. Baranovskii, S. Yamasaki, K. Ikuta, K. Tanaka, M. Kondo, A. Matsuda, and P. Thomas, Phys. Status Solidi **205**, 147 (1998).
[18]W. Fuhs, P. Kanschat, and K. Lips, J. Vac. Sci. Technol. B **18**, 1792 (2000).
[19]R. Brüggemann, J. Appl. Phys. **92**, 2540 (2002).
[20]H. B. T. Li, R. L. Stolk, C. H. M. van der Werf, R. H. Franken, J. K. Rath, and R. E. I. Schropp, J. Non-Cryst. Solids **352**, 1941 (2006).
[21]H. B. T. Li, R. H. Franken, R. L. Stolk, C. H. M. van der Werf, J. K. Rath, and R. E. I. Schropp, J. Non-Cryst. Solids **354**, 2087 (2008).